water

MDPI

Article

A Non-Hydrostatic Model for Simulating Weakly Dispersive Landslide-Generated Waves

Dede Tarwidi [1,2,*], Sri Redjeki Pudjaprasetya [1] and Sugih Sudharma Tjandra [3]

[1] Industrial and Financial Mathematics Research Group, Faculty of Mathematics and Natural Sciences, Institut Teknologi Bandung, Jalan Ganesha No. 10, Bandung 40132, Indonesia
[2] School of Computing, Telkom University, Jalan Telekomunikasi No. 1 Terusan Buah Batu, Bandung 40257, Indonesia
[3] Industrial Engineering, Parahyangan Catholic University, Jalan Ciumbuleuit No. 94, Bandung 40141, Indonesia
* Correspondence: dedetarwidi@telkomuniversity.ac.id

Abstract: The aim of this study is to develop an efficient numerical scheme that is capable of simulating landslide-generated waves. The numerical scheme is based on the one-layer non-hydrostatic (NH-1L) model, a phase-solving model that can account for weakly dispersive waves. In this paper, the model is extended to include a time-varying solid bed. This NH-1L scheme is very efficient because, at each time step, only a tridiagonal Poisson pressure matrix needs to be solved. In this study, the capability of the NH-1L scheme to simulate landslide-generated waves is demonstrated by executing two types of landslide motion: constant speed and with acceleration and deceleration. Validation was performed using analytical solutions of the linear weakly dispersive (LWD) model, as well as experimental data. The NH-1L model was capable of describing the generation and propagation of water waves by a submarine landslide from relatively intermediate water to shallow water depths.

Keywords: non-hydrostatic model; weakly dispersive wave; submarine landslide; tsunami

Citation: Tarwidi, D.; Pudjaprasetya, S.R.; Tjandra, S.S. A Non-Hydrostatic Model for Simulating Weakly Dispersive Landslide-Generated Waves. *Water* **2023**, *15*, 652. https://doi.org/10.3390/w15040652

Academic Editor: Roberto Greco

Received: 28 November 2022
Revised: 12 January 2023
Accepted: 2 February 2023
Published: 7 February 2023

1. Introduction

Landslide-induced tsunamis are natural disasters that can strike the coast without warning because they may not be preceded by earthquakes. Therefore, it is important to predict the magnitude and initial location of these tsunamis. Although landslide tsunamis account for only 7% of all tsunamis [1], they are nearly as destructive as earthquake-triggered tsunamis. This motivates a comprehensive study of landslide-generated waves that is necessary for the development of disaster mitigation strategies. The application of numerical models may provide solutions to these issues.

There have been several attempts to develop numerical models capable of simulating landslide tsunamis. Non-linear shallow water equations are commonly used due to their simplicity and efficiency in tsunami modeling [2–6]. However, these models are less accurate when simulating the generation of tsunamis in areas of intermediate or deep water depth, where the dispersion effects are fairly significant. Other models that integrate non-linear and dispersion effects are Boussinesq-type wave equations [7–11] and potential flow equations [12–14]. However, numerical approaches to Boussinesq-type models are difficult to implement due to the presence of mixed high-order derivative variables, while the application of potential flow models is restricted by the assumption of ideal fluids and irrotational motion [15]. Moreover, the other widely used dispersive models for landslide-generated tsunamis are based on the Navier–Stokes equations [16–20]. Unfortunately, due to their computational complexity, these models are costly to calculate.

The non-hydrostatic model is a wave model derived from the Navier–Stokes equations with hydrodynamic pressure along the flow depth [21–25]. The efficiency and accuracy of

wave dispersion characteristics are the main focus in developing non-hydrostatic models. In this case, the non-hydrostatic model trades off accuracy for efficiency; accuracy may be improved by utilizing more vertical layers of the fluid flow, but efficiency is achieved by employing fewer layers. Stelling and Zijlema [26] showed that a non-hydrostatic model with two vertical layers might approximate the dispersion relation up to $kd_0 \approx 9.7$, with an error of around 3%, where k and d_0 are the wave number and undisturbed water depth, respectively. Several attempts have been made to enhance the efficiency of non-hydrostatic models while preserving the necessary level of accuracy. Bai and Cheung [27] proposed that the non-hydrostatic pressure at the half depth of the two-layer model should be described in terms of the pressure of the bottom layer with an independent parameter. The efficiency achieved by employing this approach is comparable to that of a one-layer non-hydrostatic model. In addition, Cui et al. [28] suggested that the horizontal velocity in the bottom layer could be expressed with a simple stencil, thus eliminating the need to calculate the vertical velocity and pressure at the bottom. This approach has yielded a Poisson pressure equation equivalent to that of the one-layer model, but with a degree of accuracy comparable to that of the two-layer model. Tarwidi et al. [29] have recently extended the reduced two-layer model of Cui et al. [28] to include a time-varying solid bottom, allowing it to correctly simulate landslide-induced tsunamis. Several comparisons with experimental results on submarine landslides have shown the validity of this model. However, the drawback of the model is its dependence on two independent parameters that must be determined before implementation.

In real-world tsunami simulations, large spatial domains with high resolution are frequently employed. In this situation, the efficiency of the numerical models is the main issue. To achieve the desired efficiency, tsunami dispersion effects are frequently approximated using a non-hydrostatic model with a single layer, which is accurate up to $kd_0 \approx 3$ within an error of 3% [30]. This study aims to show that the one-layer non-hydrostatic model can accurately simulate landslide-generated waves where the ratio of the water depth to the landslide length is relatively small; in other words, the generated waves have weakly dispersive effects. Here, we adopt the well-known staggered-grid finite-volume method due to its accuracy and simplicity in solving the non-linear and dispersive model. To examine the capabilities of the one-layer model for simulating landslide-generated tsunamis, we perform a series of numerical simulations and validate the results using analytical and laboratory experiment results. The present study is one of the first attempts to thoroughly examine the one-layer model for simulating tsunamis generated by landslides and may lay the groundwork for future research into more complex problems.

This paper is structured as follows: Section 2 gives a brief overview of the full governing equations of the one-layer non-hydrostatic model and its associated numerical techniques. Section 3 discusses the validation of the numerical scheme for the landslide motion with constant speed and acceleration using analytical solutions. The third section also describes the validation of the numerical model with experimental results. Lastly, Section 4 provides a summary of the main significant results of the study.

2. Governing Equations and the NH-1L Scheme

This section presents the one-layer non-hydrostatic model (also referred to simply as NH-1L), which is used in this article to simulate the waves generated by landslides. Next, we discuss the numerical implementation using the finite-volume approach on a staggered grid.

The governing equations of the one-layer non-hydrostatic model are based on the Euler equations. Let Ω be a fluid domain, bounded by the free surface $z = \eta(x,t)$ and the time-varying bathymetry $z = -d(x,t)$. The total fluid thickness is given by $h(x,t) = \eta(x,t) + d(x,t)$. Moreover, the horizontal velocity of the fluid is denoted by $u(x,t)$. Meanwhile, the vertical velocity on the free surface and the moving bottom is represented by $w_{\text{top}}(x,t)$ and $w_{\text{bot}}(x,t)$, respectively. On the free surface, the hydrodynamic

pressure is zero, whereas, at the bottom, it is indicated by $q(x,t)$. Figure 1 illustrates the variables used in the NH-1L model.

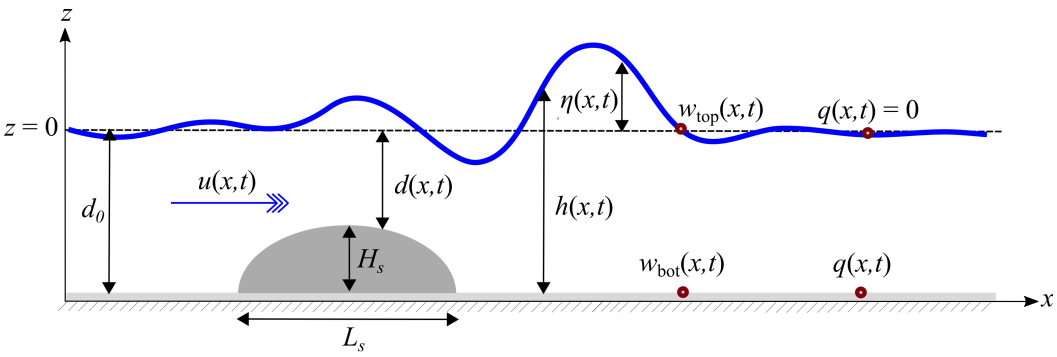

Figure 1. Variables in a one-layer non-hydrostatic model.

The one-layer non-hydrostatic model is given by the following equations:

$$\frac{\partial h}{\partial t} + \frac{\partial (hu)}{\partial x} = 0, \tag{1}$$

$$\frac{\partial u}{\partial t} + u\frac{\partial u}{\partial x} + g\frac{\partial \eta}{\partial x} = -\frac{1}{2}\frac{\partial q}{\partial x}, \tag{2}$$

$$\frac{1}{2}\left(\frac{\partial w_{\text{top}}}{\partial t} + \frac{\partial w_{\text{bot}}}{\partial t}\right) = \frac{q}{h}, \tag{3}$$

$$\frac{w_{\text{top}} - w_{\text{bot}}}{h} + \frac{\partial u}{\partial x} = 0, \tag{4}$$

$$w_{\text{bot}} = -\frac{\partial d}{\partial t} - u\frac{\partial d}{\partial x}, \tag{5}$$

where g is the gravitational acceleration. Equation (1) is the conservation of mass. Equations (2) and (3) are the momentum balance in the horizontal and vertical directions, respectively. Equation (4) is the depth-integrated continuity equation. More details on the derivation of Equations (1)–(4) can be found in Pudjaprasetya et al. [31]. In this article, we intend to simulate landslide-generated waves, i.e., involving a moving base, so here the kinematic equation of the base is formulated as Equation (5), with $d(x,t)$ representing the time-varying bottom.

The NH-1L model has five equations and five unknowns, namely $h, u, w_{\text{top}}, w_{\text{bot}}$, and q. After excluding all non-linear terms in Equations (1)–(5), the dispersion relation of the linear system is given by

$$\left(\frac{\omega}{k}\right)^2 = c^2 = gd_0\frac{1}{1+\frac{1}{4}(kd_0)^2}, \tag{6}$$

where c is the wave speed, and ω and k are the frequency and wave number, respectively. To verify that the dispersion relation is accurate, we compare it with the exact dispersion relation, which is derived from Airy wave theory:

$$c^2_{\text{exact}} = gd_0\frac{\tanh(kd_0)}{kd_0}. \tag{7}$$

Figure 2 depicts the wave speed of the NH-1L model as a function of kd_0 compared to the exact solution. It can be seen that the NH-1L model produces an accurate dispersion relation up to $kd_0 \approx 3$, with a relative error of 3%, whereas the dispersive curve of the Boussinesq model of Nwogu [32] approximates the exact dispersion curve up to $kd_0 \approx 4$, with a relative error of 3%. This demonstrates that our NH-1L model has a dispersion relation comparable to that of the Boussinesq model of Nwogu [32]. Moreover, the dispersion curve of the two-layer non-hydrostatic model (NH-2L) model is also shown in Figure 2,

which clearly shows that the curve accurately approximates the exact dispersion up to $kd_0 \approx 10$.

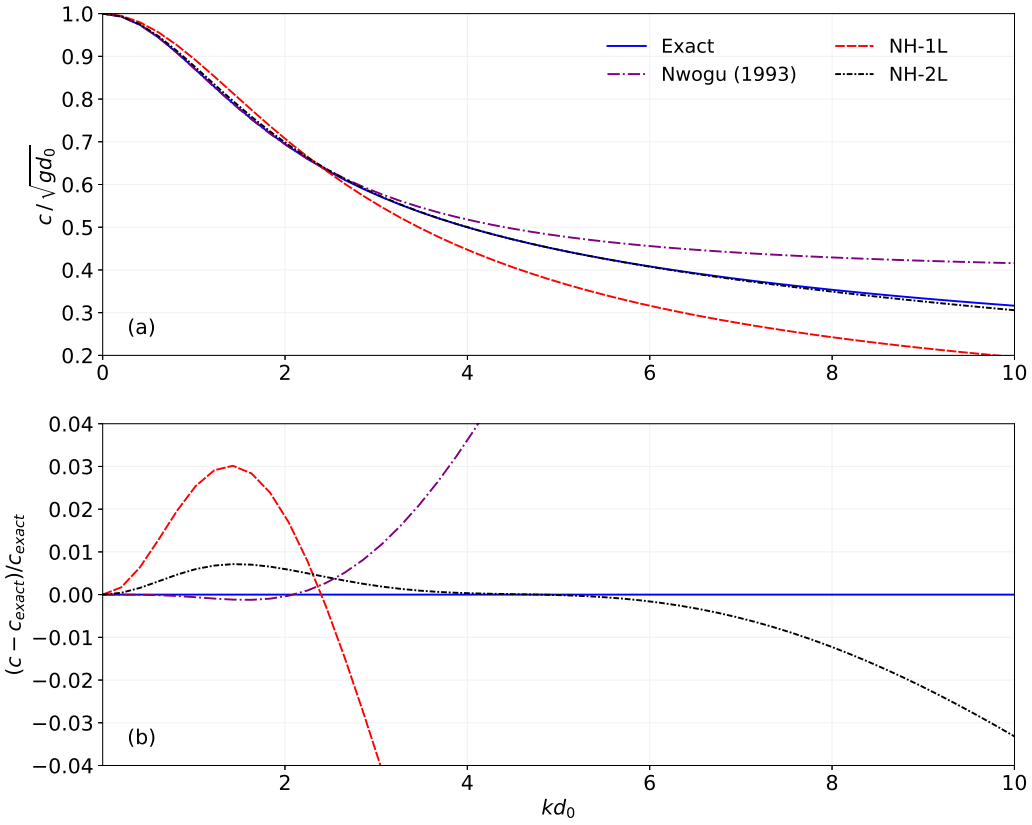

Figure 2. (**a**) Wave speed normalized by $\sqrt{gd_0}$ as a function of kd_0. (**b**) Relative error of the wave speed.

We numerically solve the NH-1L model using the finite-volume method on a staggered grid. Consider the computational domain of $l_1 \leq x \leq l_2$ and $0 \leq t \leq T$. The spatial domain $[l_1, l_2]$ is divided into uniform sub-intervals, with a step size of $\Delta x/2$, and the time domain $[0, T]$, with a step size of Δt. The grid points along the spatial domain are as follows $x_{1/2} = l_1, x_1, x_{3/2}, \cdots, x_{j-1/2} = (j-1/2)\Delta x, x_j, x_{j+1/2} = (j+1/2)\Delta x, \cdots, x_{N_x}, x_{N_x+1/2} = l_2$, with $N_x = (l_2 - l_1)/\Delta x$. The dependent variable $u(x,t)$ is evaluated at half grid points $x_{j+1/2}$, while $h(x,t)$ (and hence $\eta(x,t)$) is calculated at the full grid points x_j. Their notations at any time step $t^n = n\Delta t$ are $u^n_{j+1/2}$, h^n_j, and η^n_j, respectively. Other variables are approximated at the full grid points, as follows: q^n_j, h^n_j, $w^n_{\text{top},j}$, and $w^n_{\text{bot},j}$ (see Figure 3 for an illustration).

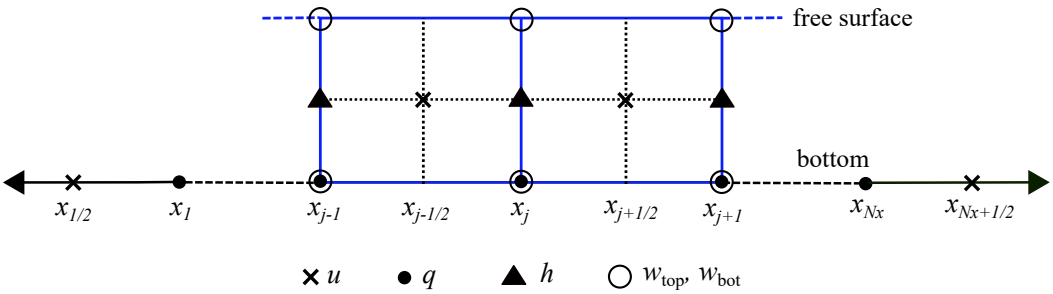

Figure 3. Staggered grid partition with locations of the unknown variables in the one-layer non-hydrostatic model.

Using the discretization of the staggered grid, the numerical scheme of the NH-1L model is expressed as

$$\frac{h_j^{n+1}-h_j^n}{\Delta t}+\frac{{}^*h_{j+\frac{1}{2}}^n u_{1,j+\frac{1}{2}}^n-{}^*h_{j-\frac{1}{2}}^n u_{1,j-\frac{1}{2}}^n}{\Delta x}=0, \tag{8}$$

$$\frac{u_{j+\frac{1}{2}}^{n+1}-u_{j+\frac{1}{2}}^n}{\Delta t}+u\frac{\partial u}{\partial x}\bigg|_{j+\frac{1}{2}}^n+g\frac{\eta_{j+1}^{n+1}-\eta_j^{n+1}}{\Delta x}=-\frac{q_{j+1}^{n+1}-q_j^{n+1}}{2\Delta x}, \tag{9}$$

$$w_{\mathrm{top},j}^{n+1}=w_{\mathrm{top},j}^n+\frac{2\Delta t}{h_j^{n+1}}q_j^{n+1}-w_{\mathrm{bot},j}^{n+1}+w_{\mathrm{bot},j}^n, \tag{10}$$

$$w_{\mathrm{top},j}^{n+1}+h_j^{n+1}\frac{u_{j+\frac{1}{2}}^{n+1}-u_{j-\frac{1}{2}}^{n+1}}{\Delta x}=w_{\mathrm{bot},j}^{n+1}, \tag{11}$$

$$w_{\mathrm{bot},j}^{n+1}=-\frac{d_j^{n+1}-d_j^n}{\Delta t}-\max\left\{0,u_{j-\frac{1}{2}}^n\right\}\frac{d_j^n-d_{j-1}^n}{\Delta x}-\min\left\{0,u_{j+\frac{1}{2}}^n\right\}\frac{d_{j+1}^n-d_j^n}{\Delta x}, \tag{12}$$

where ${}^*h_{j+\frac{1}{2}}^n$ is obtained by the following upwind approximation:

$${}^*h_{j+\frac{1}{2}}=\begin{cases}h_j, & u_{j+\frac{1}{2}}>0,\\ h_{j+1}, & u_{j+\frac{1}{2}}<0,\\ \max\{\eta_j,\eta_{j+1}\}+\min\{d_j,d_{j+1}\}, & u_{j+\frac{1}{2}}=0.\end{cases} \tag{13}$$

In Equation (9), the advection term is approximated by

$$u\frac{\partial u}{\partial x}\bigg|_{j+\frac{1}{2}}^n=\frac{1}{\bar{h}_{j+\frac{1}{2}}}\left(\frac{\bar{r}_{j+1}\,{}^*u_{j+1}-\bar{r}_j\,{}^*u_j}{\Delta x}-u_{j+\frac{1}{2}}\frac{\bar{r}_{j+1}-\bar{r}_j}{\Delta x}\right), \tag{14}$$

where

$$\bar{h}_{j+\frac{1}{2}}=\frac{1}{2}(h_j+h_{j+1}),\quad \bar{r}_j=\frac{1}{2}(r_{j+\frac{1}{2}}-r_{j-\frac{1}{2}}),$$
$$r_{j+\frac{1}{2}}={}^*h_{j+\frac{1}{2}}u_{j+\frac{1}{2}},\quad {}^*u_j=\begin{cases}u_{j-\frac{1}{2}}, & \bar{r}_j\geq 0,\\ u_{j+\frac{1}{2}}, & \bar{r}_j<0.\end{cases} \tag{15}$$

Equations (8)–(12) contain the unknown variable q^{n+1}. To obtain the solution of this variable, substituting Equations (9) and (10) into Equation (11) yields the Poisson pressure equation as follows:

$$\begin{bmatrix}b_1 & c_1 & & & 0\\ a_2 & b_2 & c_2 & & \\ & \ddots & \ddots & \ddots & \\ & & a_{N_x-1} & b_{N_x-1} & c_{N_x-1}\\ 0 & & & a_{N_x} & b_{N_x}\end{bmatrix}\begin{bmatrix}q_1^{n+1}\\ q_2^{n+1}\\ \vdots\\ q_{N_x-1}^{n+1}\\ q_{N_x}^{n+1}\end{bmatrix}=\begin{bmatrix}f_1\\ f_2\\ \vdots\\ f_{N_x-1}\\ f_{N_x}\end{bmatrix}, \tag{16}$$

where

$$a_i=-\frac{\Delta t}{2\Delta x}h_j^{n+1},\quad b_i=\frac{\Delta t}{\Delta x}h_j^{n+1}+\frac{2\Delta x\Delta t}{h_j^{n+1}},\quad c_i=-\frac{\Delta t}{2\Delta x}h_j^{n+1}, \tag{17}$$

$$f_i=-h_j^{n+1}\left(\hat{u}_{j+\frac{1}{2}}-\hat{u}_{j-\frac{1}{2}}\right)-\Delta x\left(w_{\mathrm{top},j}^n+w_{\mathrm{bot},j}^n\right)+2\Delta x\,w_{\mathrm{bot},j}^{n+1}. \tag{18}$$

Equation (16) is a system of linear equations with a tridiagonal matrix coefficient, which is then solved using Thomas's algorithm; hence, it is very efficient. Whereas the NH-

2L model requires solving a pentadiagonal matrix at each time step, it is the trade-off from the NH-2L model that performs better in terms of dispersion (Figure 2). More discussion about the NH-2L model can be found in Pudjaprasetya et al. [31].

We calculate $u_{j+1/2}$ at each time step using the predictor–corrector approach. In the predictor phase, $u_{j+1/2}$ is determined by solving Equation (9) with zero hydrodynamic pressure. The predicted value obtained from the predictor step is denoted by $\hat{u}_{j+1/2}$. Furthermore, in the corrector step, we apply a correction to the predicted value by

$$u_{j+\frac{1}{2}}^{n+1} = \hat{u}_{j+\frac{1}{2}} - \Delta t \frac{q_{j+1}^{n+1} - q_j^{n+1}}{2\Delta x}. \tag{19}$$

The computational method for the NH-1L model is summarized as follows.

1. Calculate h^{n+1} from Equation (8); then the free surface is $\eta^{n+1} = h^{n+1} - d^{n+1}$.
2. Calculate $\hat{u}$ using Equation (9), where the non-hydrostatic pressure term is neglected.
3. Solve the linear system of Equation (16) to obtain q^{n+1}.
4. Calculate w_{bot}^{n+1} using Equation (12).
5. Calculate the corrected values of u^{n+1} using Equation (19).
6. Calculate w_{top}^{n+1} using Equation (10).

3. Model Validation

In this section, the NH-1L model is validated using analytical solutions and experimental results. Two different landslide motions are considered: with constant speed in Section 3.1, and with acceleration and deceleration in Section 3.2. In doing this, we first define the dimensionless variables as follows:

$$\hat{x} = \frac{x}{L_s}, \quad \hat{t} = t\sqrt{\frac{g}{L_s}}, \quad \hat{\eta} = \frac{\eta}{H_s}, \tag{20}$$

and the dimensionless parameters:

$$\lambda = \frac{a_0}{g}, \quad Fr = \frac{u_t}{\sqrt{g d_0}}, \quad \mu = \frac{d_0}{L_s}. \tag{21}$$

Here, λ denotes the dimensionless landslide acceleration, Fr is the Froude number, and μ represents the ratio between the water depth and the landslide length—it is often referred to as the dispersion parameter.

3.1. Waves Generated by Landslide with Constant Speed

Consider a Gaussian-shaped landslide moving horizontally with constant speed u_t at a constant water depth d_0. The bottom motion is given by

$$d(x,t) = d_0 - H_s e^{-\frac{1}{2}(x-u_t t)^2}, \tag{22}$$

where the length and the maximum thickness of the landslide are $L_s = 4$ m and $H_s = 1$ m, respectively. In the beginning, the water surface and the landslide were both at rest. Simulations were carried out using the NH-1L numerical scheme in which the advection term is ignored; here, we use $\Delta x = 0.05$ m and $\Delta t = 0.05$ s for the computations.

Our numerical model is compared with two analytical solutions from Lo and Liu [33], i.e., the linear and weakly dispersive (LWD) and the linear and fully dispersive (LFD) models. These analytical solutions are structured as the sum of three different waves: η_+, η_-, and η_{Fr}. The first two waves η_+ and η_- have the same wave speed but travel in opposite directions; in addition, their shapes may change over time due to frequency dispersion. Meanwhile, the last wave component η_{Fr} moves with the speed of the landslide and maintains its shape. For this assessment, we perform simulations with five different dispersion parameters $\mu \in [0.1, 0.5]$, whereas the Froude number is kept constant $Fr = 0.375$.

Figure 4 shows the contour plots of the water surface obtained from three different models: the numerical model NH-1L and two analytical wave models LWD and LFD, for $\mu = 0.1, 0.2$. The wave contours are plotted on the normalized spatial and temporal axes; the color bar represents the normalized wave amplitudes. As seen in Figure 4, in response to the landslide motion at the bottom, three distinct waves emerge from $x/L_s = 0$ and then separate over time; one positive hump and one negative trough propagate with the same speed to the right and left, respectively. At the same time, one trough propagates with landslide speed u_t to the right. Figure 4 shows that the surface waves generated by the NH-1L model confirm the three-wave structure of the analytical solutions of LWD and LFD. In this case, the leading wave travels at approximately the shallow water wave celerity $\sqrt{gd_0}$, represented by the dashed lines in the figure. In addition, Figure 5 shows the wave profiles at a certain time $t\sqrt{g/L_s} = 12$. For a relatively small dispersion parameter $\mu = 0.1$, the results of NH-1L, LFD, and LFD are nearly identical to the solution of the linear shallow water equation (LSWE). Furthermore, for the somewhat larger dispersion parameter $\mu = 0.2$, the NH-1L model can still give results comparable to the dispersive solutions of the LWD and LFD models.

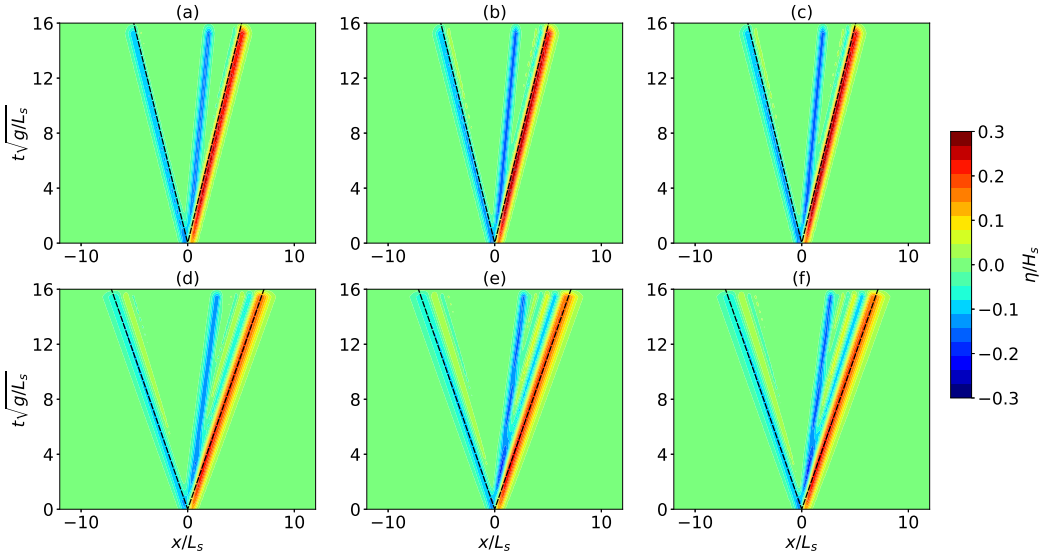

Figure 4. Comparison of the wave-field contours obtained from three different wave models: (**a**,**d**) NH-1L model, (**b**,**e**) LWD model, (**c**,**f**) LFD model, for (**a**–**c**) $\mu = 0.1$, (**d**–**f**) $\mu = 0.2$. The dashed line represents the characteristic curves with wave celerity $\pm\sqrt{gd_0}$.

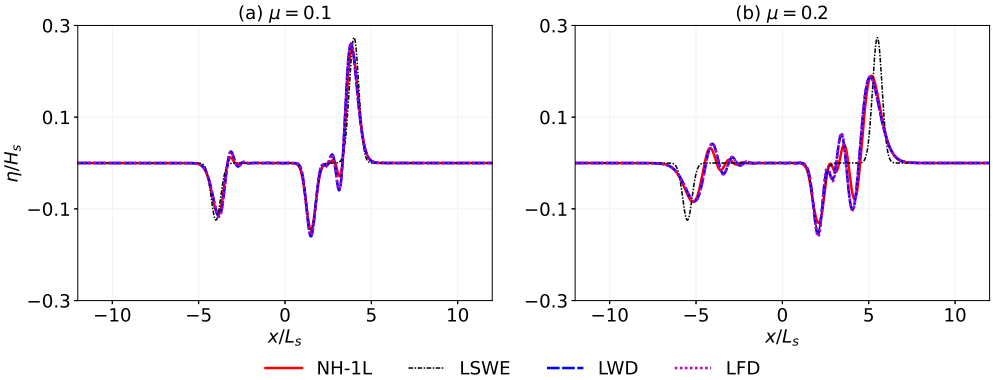

Figure 5. The free surface profiles at time $t\sqrt{g/L_s} = 12$ resulting from the NH-1L simulation are compared with the LSWE, LWD, and LFD models for two dispersion parameters (**a**) $\mu = 0.1$. (**b**) $\mu = 0.2$.

The wave-field contours for higher dispersion parameters ($\mu = 0.3, 0.4$) are depicted in Figure 6, while the free surface profiles for time $t\sqrt{g/L_s} = 12$ are presented in Figure 7. It can be seen that each of the three wave groups has a leading wave followed by tailing waves as a result of the dispersive effects. For $\mu = 0.3$, the NH-1L model accurately simulates the landslide-generated waves; the numerical results agree well with those obtained by LWD and LFD models. Moreover, for $\mu = 0.4$, the NH-1L model is still quite close to the LWD and LFD models, but starts to produce higher oscillating tails behind the leading wave.

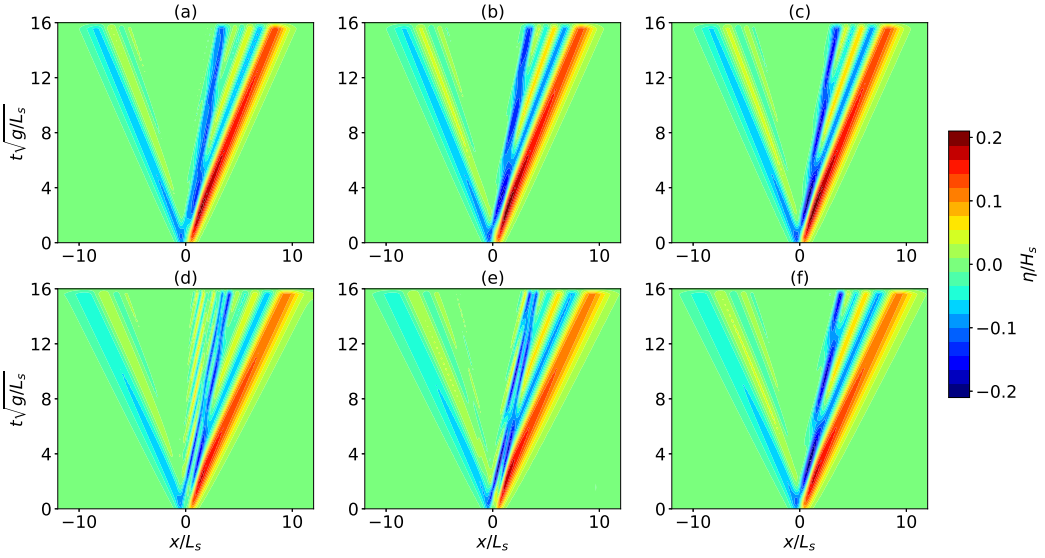

Figure 6. Comparison of wave-field contours obtained from three different wave models: (**a**,**d**) NH-1L model. (**b**,**e**) LWD model. (**c**,**f**) LFD model. (**a**–**c**) $\mu = 0.3$. (**d**–**f**) $\mu = 0.4$. The dashed lines represent the characteristic curves with wave celerity $\pm\sqrt{gd_0}$.

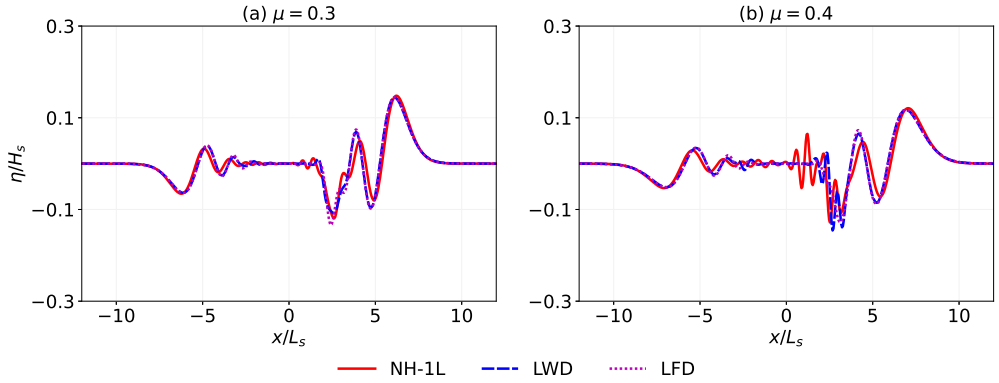

Figure 7. The free surface profiles at time $t\sqrt{g/L_s} = 12$ resulting from the NH-1L simulation are compared with the LWD and LFD models for two dispersion parameters (**a**) $\mu = 0.3$. (**b**) $\mu = 0.4$.

The calculation result of the NH-1L model for $\mu = 0.5$ is presented in Figure 8, where the water level is plotted together with the results of the LWD and LFD models. Figure 9 depicts the wave-field contours that resulted from the three models NH-1L, LWD, and LFD. It can be seen from both figures that, for the dispersion parameter $\mu = 0.5$, the simulation with the NH-1L scheme produces a lot of wiggles behind the main wave. It indicates that, for $\mu = 0.5$, the NH-1L scheme is no longer valid. These results suggest that the NH-1L model is suitable for landslide simulations within the range of dispersion parameters of $0 < \mu < 0.4$, which is in the range of intermediate to shallow water. Moreover, in the next subsection, we show that the NH-1L model is still accurate compared to the existing experimental data, a case that corresponds to $\mu = 0.35$.

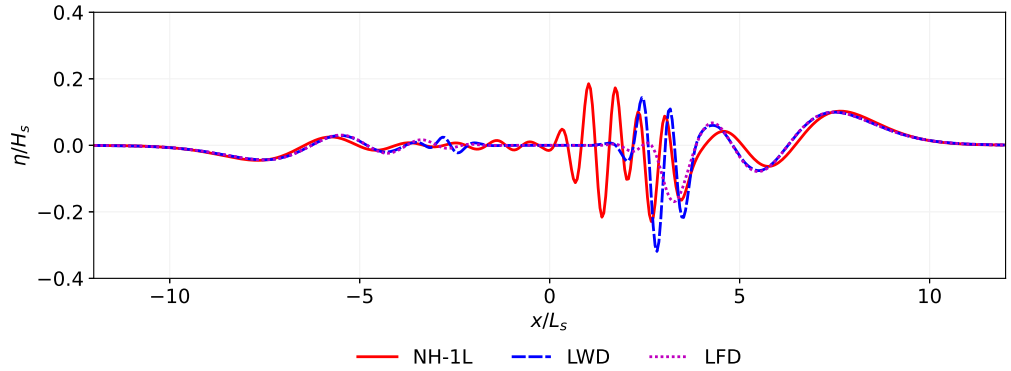

Figure 8. Free surface profiles at time $t\sqrt{g/L_s} = 12$ resulting from the NH-1L simulation are compared with the LWD and LFD models for the dispersion parameter $\mu = 0.5$.

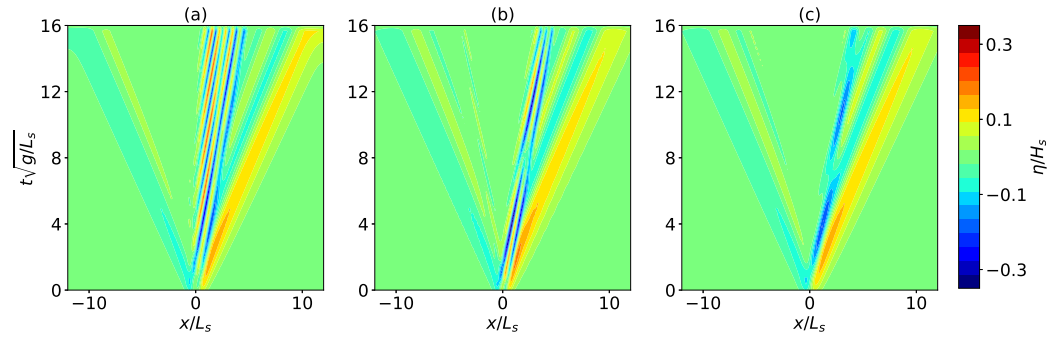

Figure 9. Comparison of wave-field contours obtained by different models with the $\mu = 0.5$: (**a**) NH-1L model. (**b**) LWD model. (**c**) LFD model.

3.2. Waves Generated by Landslide with Acceleration

In this section, we validate the NH-1L scheme using some experimental results from Whittaker et al. [34]. Their experiments used a moving semi-elliptical block as a submarine landslide on a flat bottom. As presented in Jing et al. [35], the time-varying topography can be expressed as

$$d(x,t) = d_0 - H_s\left[1 - \left(\frac{2(x - S(t))}{L_s}\right)^4\right], \quad -\frac{L_s}{2} + S(t) < x < \frac{L_s}{2} + S(t), \tag{23}$$

where $H_s = 0.026$ m and $L_s = 0.5$ m are the maximum thickness and the length of the landslide, respectively. Here, the landslide motion $S(t)$ is given by

$$S(t) = \begin{cases} \frac{1}{2}a_0t^2, & 0 \le t \le t_1 \\ \frac{1}{2}a_0t_1^2 + u_t(t - t_1), & t_1 < t \le t_2 \\ \frac{1}{2}a_0t_1^2 + u_t(t_2 - t_1) + u_t(t - t_2) - \frac{1}{2}a_0(t - t_2)^2, & t_2 < t \le t_3 \\ \frac{1}{2}a_0t_1^2 + u_t(t_2 - t_1) + u_t(t_3 - t_2) - \frac{1}{2}a_0(t_3 - t_2)^2, & t > t_3 \end{cases} \tag{24}$$

where

$$t_1 = \frac{u_t}{a_0}, \quad t_2 = t_1 + 2, \quad t_3 = t_2 + t_1, \tag{25}$$

a_0 and u_t are the initial acceleration of the landslide and the maximum velocity of the landslide, respectively.

From a number of experiments conducted by Whittaker et al. [34], we select the experimental results of run 21, run 23, and run 12 to validate our NH-1L model, namely Equations (8)–(12). The dimensionless parameters used in this experiment are summarized

in Table 1. Here, we also compare the results of the NH-1L model with the analytical solutions of Jing et al. [35].

Table 1. Dimensionless parameters used in the landslide experiment of Whittaker et al. [34].

Run	λ	Fr	μ
21	0.153	0.125	0.35
23	0.153	0.375	0.35
12	0.102	0.500	0.70

We begin with a numerical simulation using the parameters of run 21. The landslide experienced a constant acceleration of $a_0 = 1.5$ m/s^2 during the first 0.109 s, followed by a constant speed of $u_t = 0.164$ m/s until a time of $t = 2.109$ s. The landslide started to decelerate and finally came to rest at $t = 2.218$ s. Snapshots of free surface waves generated from this landslide motion are shown in Figure 10, in which we compare the results of the NH-1L model, the LWD model [35], and laboratory experiments [34] at subsequent times. In the simulation of run 21 using parameters $\lambda = 0.153$, $\mu = 0.35$, and $Fr = 0.125$, the calculation of the NH-1L scheme shows good agreement with the LWD results and the experimental data. However, when the landslide motion has stopped at $t\sqrt{g/L_s} = 13.79$, the resulting wave calculated by the NH-1L model is slightly higher than the experimental results.

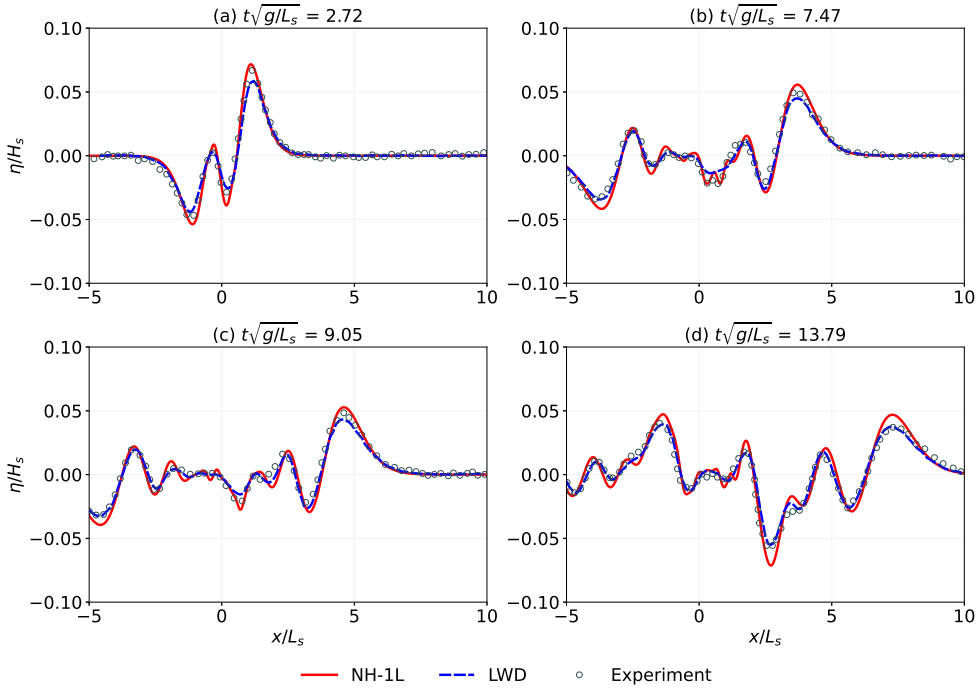

Figure 10. Wave profiles at subsequent times from run 21; results of the NH-1L model are compared with the LWD and experimental data.

Figure 11 shows the results of the subsequent calculations using the run 23 parameters. Although it has the same acceleration, the speed of the landslide in run 23 is three times faster than in run 21. The parameter values for this simulation are $\lambda = 0.153$, $\mu = 0.35$, and $Fr = 0.375$. As shown in Figure 11, the NH-1L results match the measurement data, while the LWD model generates slightly lower waves. In this case, to account for increased landslide velocities, a non-linear numerical model is required, as described by Jing et al. [35]. Figures 10 and 11 confirm that the NH-1L model can still provide results that are comparable to the experimental data for the case of the dispersion parameter $\mu = 0.35$.

Furthermore, we perform the calculation using parameters of run 12, which correspond to $\mu = 0.7$; as shown in Figure 12, the NH-1L model failed to simulate this highly dispersive case, and the LWD model also failed. Both weakly dispersive models, the NH-1L and the LWD, overpredict the amplitude and shape of the generated waves. For this case, we require a better non-hydrostatic model with a broader dispersion range, such as the two-layer non-hydrostatic model (NH-2L). Figure 12 also depicts the results of the calculations performed with the NH-2L model. We can see that the NH-2L model can clearly simulate the run 12 case better than the weakly dispersive NH-1L model.

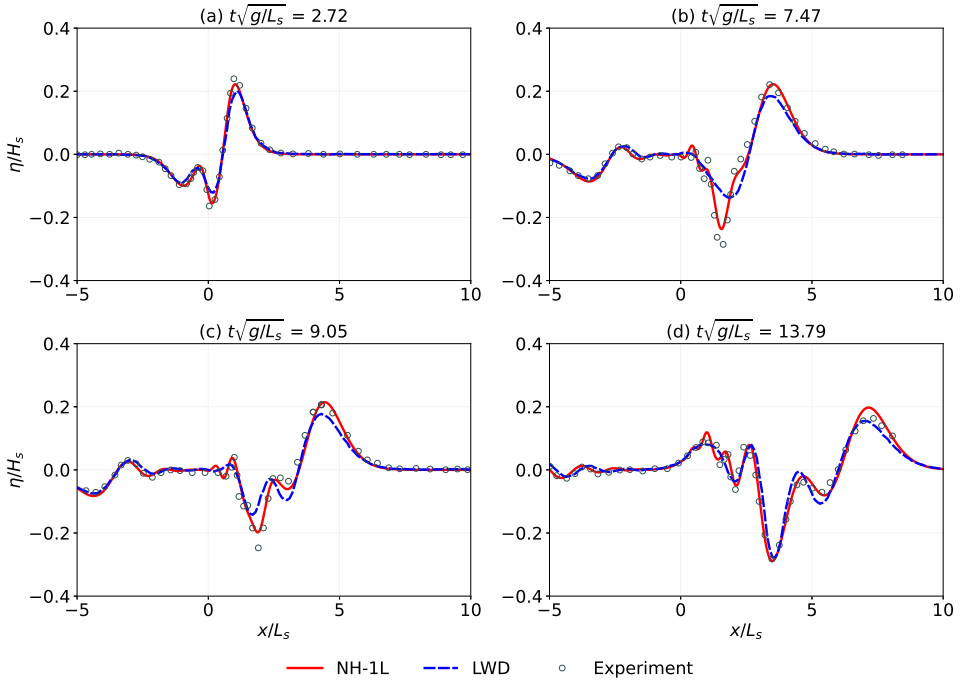

Figure 11. Comparisons of observed and predicted wave heights at several times in run 23.

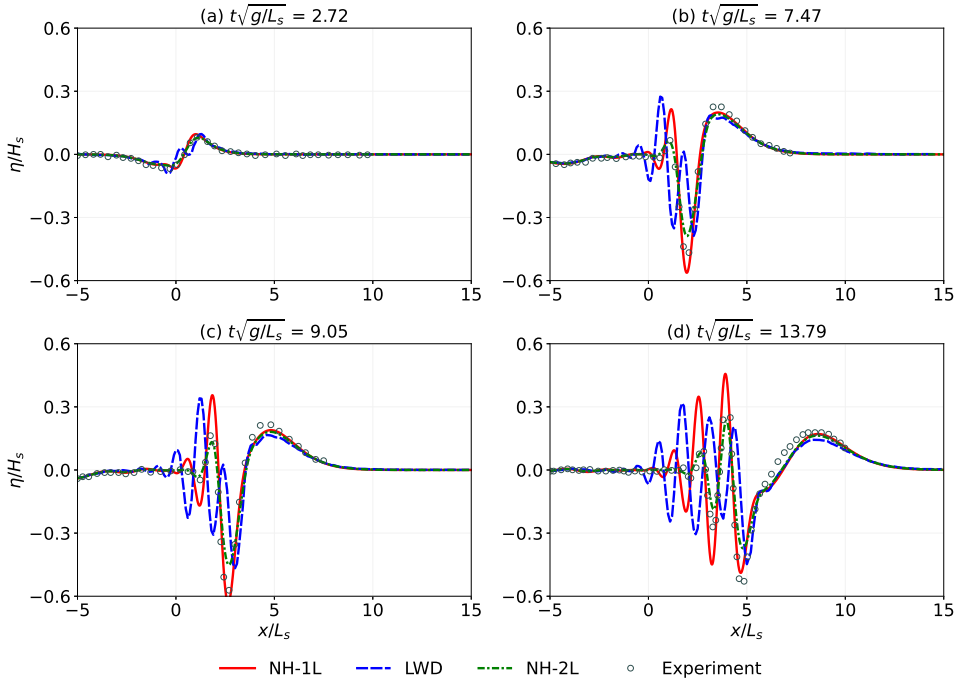

Figure 12. Comparisons of observed and predicted wave heights at several times in run 12.

4. Conclusions

We have developed an efficient numerical scheme that is capable of simulating waves generated by landslides, which is called the one-layer non-hydrostatic model (NH-1L). We used the scheme to simulate the appearance of free-surface deformation caused by landslide motions: landslides moving at constant speed on a flat bottom and landslides moving with acceleration. Our numerical NH-1L results show good agreement with the results of the linear weakly dispersive model (LWD), as well as the experimental results of Whittaker et al. [34] and, therefore, provide good validation for the NH-1L scheme. The proposed numerical scheme has several positive properties, including the following: the scheme is relatively simple and adopts the bottom movement directly, and the scheme is efficient because each time step only needs to solve the equation with a tridiagonal Poisson matrix. Further evaluation shows that the NH-1L model is a feasible alternative to tsunami modeling due to its ability to simulate weakly dispersive landslide-generated waves from relatively intermediate to shallow water depths.

Author Contributions: Conceptualization, S.R.P. and D.T.; methodology, S.R.P. and S.S.T.; software, D.T.; validation, D.T. and S.R.P.; formal analysis, S.R.P. and S.S.T.; investigation, S.S.T.; writing—original draft preparation, D.T. and S.R.P.; writing—review and editing, S.R.P. and S.S.T.; visualization, D.T.; funding acquisition, S.R.P. All authors have read and agreed to the published version of the manuscript.

Funding: This research received no external funding. The APC was funded by Telkom University.

Data Availability Statement: Not applicable.

Acknowledgments: This research is part of the dissertation research of Dede Tarwidi, funded by Telkom Foundation/Telkom University. Dede Tarwidi is grateful for the Telkom University Scholarship that supported his doctoral study at Institut Teknologi Bandung.

Conflicts of Interest: The authors declare no conflict of interest.

References

1. Harbitz, C.B.; Løvholt, F.; Bungum, H. Submarine landslide tsunamis: How extreme and how likely? *Nat. Hazards* **2014**, *72*, 1341–1374. [CrossRef]
2. Pakoksung, K.; Suppasri, A.; Imamura, F.; Athanasius, C.; Omang, A.; Muhari, A. Simulation of the Submarine Landslide Tsunami on 28 September 2018 in Palu Bay, Sulawesi Island, Indonesia, Using a Two-Layer Model. *Pure Appl. Geophys.* **2019**, *176*, 3323–3350. [CrossRef]
3. González-Vida, J.M.; Macías, J.; Castro, M.J.; Sánchez-Linares, C.; de la Asunción, M.; Ortega-Acosta, S.; Arcas, D. The Lituya Bay landslide-generated mega-tsunami—Numerical simulation and sensitivity analysis. *Nat. Hazards Earth Syst. Sci.* **2019**, *19*, 369–388. [CrossRef]
4. Paris, A.; Heinrich, P.; Paris, R.; Abadie, S. The December 22, 2018 Anak Krakatau, Indonesia, Landslide and Tsunami: Preliminary Modeling Results. *Pure Appl. Geophys.* **2020**, *177*, 571–590. [CrossRef]
5. Liu, Q.; Pan, M.; Wang, X.; An, Y. A two-layer model for landslide generated impulse wave: Simulation of the 1958 Lituya bay landslide impact wave from generation to long–duration transport. *Adv. Water Resour.* **2021**, *154*, 103989. [CrossRef]
6. Mungkasi, S.; Magdalena, I.; Pudjaprasetya, S.R.; Wiryanto, L.H.; Roberts, S.G. A staggered method for the shallow water equations involving varying channel width and topography. *Int. J. Multiscale Comput. Eng.* **2018**, *16*, 231–244. [CrossRef]
7. Ataie-Ashtiani, B.; Jilani, A.N. A higher-order Boussinesq-type model with moving bottom boundary: Applications to submarine landslide tsunami waves. *Int. J. Numer. Methods Fluids* **2007**, *53*, 1019–1048. [CrossRef]
8. Fuhrman, D.R.; Madsen, P.A. Tsunami generation, propagation, and run-up with a high-order Boussinesq model. *Coast. Eng.* **2009**, *56*, 747–758. [CrossRef]
9. Fang, K.; Liu, Z.; Sun, J.; Xie, Z.; Zheng, Z. Development and validation of a two-layer Boussinesq model for simulating free surface waves generated by bottom motion. *Appl. Ocean. Res.* **2020**, *94*, 101977. [CrossRef]
10. Gao, J.; Ma, X.; Zang, J.; Dong, G.; Ma, X.; Zhu, Y.; Zhou, L. Numerical investigation of harbor oscillations induced by focused transient wave groups. *Coast. Eng.* **2020**, *158*, 103670. [CrossRef]
11. Gao, J.; Ma, X.; Dong, G.; Chen, H.; Liu, Q.; Zang, J. Investigation on the effects of Bragg reflection on harbor oscillations. *Coast. Eng.* **2021**, *170*, 103977. [CrossRef]
12. Grilli, S.T.; Watts, P. Modeling of waves generated by a moving submerged body. Applications to underwater landslides. *Eng. Anal. Bound. Elem.* **1999**, *23*, 645–656. [CrossRef]

13. Grilli, S.T.; Vogelmann, S.; Watts, P. Development of a 3D numerical wave tank for modeling tsunami generation by underwater landslides. *Eng. Anal. Bound. Elem.* **2002**, *26*, 301–313. [CrossRef]
14. Grilli, S.T.; Watts, P. Tsunami Generation by Submarine Mass Failure. I: Modeling, Experimental Validation, and Sensitivity Analyses. *J. Waterw. Port Coastal Ocean. Eng.* **2005**, *131*, 283–297. .:6(283). [CrossRef]
15. Ai, C.; Ma, Y.; Yuan, C.; Xie, Z.; Dong, G. A three-dimensional non-hydrostatic model for tsunami waves generated by submarine landslides. *Appl. Math. Model.* **2021**, *96*, 1–19. [CrossRef]
16. Abadie, S.; Morichon, D.; Grilli, S.; Glockner, S. Numerical simulation of waves generated by landslides using a multiple-fluid Navier–Stokes model. *Coast. Eng.* **2010**, *57*, 779–794. [CrossRef]
17. Mao, J.; Zhao, L.; Liu, X.; Cheng, J.; Avital, E. A three-phases model for the simulation of landslide-generated waves using the improved conservative level set method. *Comput. Fluids* **2017**, *159*, 243–253. [CrossRef]
18. Li, G.; Chen, G.; Li, P.; Jing, H. Efficient and Accurate 3-D Numerical Modelling of Landslide Tsunami. *Water* **2019**, *11*, 2033. [CrossRef]
19. Paris, A.; Heinrich, P.; Abadie, S. Landslide tsunamis: Comparison between depth-averaged and Navier–Stokes models. *Coast. Eng.* **2021**, *170*, 104022. [CrossRef]
20. Kirby, J.T.; Grilli, S.T.; Horrillo, J.; Liu, P.L.F.; Nicolsky, D.; Abadie, S.; Ataie-Ashtiani, B.; Castro, M.J.; Clous, L.; Escalante, C.; et al. Validation and inter-comparison of models for landslide tsunami generation. *Ocean. Model.* **2022**, *170*, 101943. [CrossRef]
21. Ma, G.; Shi, F.; Kirby, J.T. Shock-capturing non-hydrostatic model for fully dispersive surface wave processes. *Ocean. Model.* **2012**, *43–44*, 22–35. [CrossRef]
22. Ma, G.; Kirby, J.T.; Hsu, T.J.; Shi, F. A two-layer granular landslide model for tsunami wave generation: Theory and computation. *Ocean. Model.* **2015**, *93*, 40–55. [CrossRef]
23. Young, C.C.; Wu, C.H.; Hsu, T.W. The Role of Non-Hydrostatic Effects in Nonlinear Dispersive Wave Modeling. *Water* **2020**, *12*, 3513. [CrossRef]
24. Zhang, C.; Kirby, J.T.; Shi, F.; Ma, G.; Grilli, S.T. A two-layer non-hydrostatic landslide model for tsunami generation on irregular bathymetry. 2. Numerical discretization and model validation. *Ocean. Model.* **2021**, *160*, 101769. [CrossRef]
25. Macías, J.; Escalante, C.; Castro, M.J. Multilayer-HySEA model validation for landslide-generated tsunamis—Part 1: Rigid slides. *Nat. Hazards Earth Syst. Sci.* **2021**, *21*, 775–789. [CrossRef]
26. Stelling, G.; Zijlema, M. An accurate and efficient finite-difference algorithm for non-hydrostatic free-surface flow with application to wave propagation. *Int. J. Numer. Methods Fluids* **2003**, *43*, 1–23. [CrossRef]
27. Bai, Y.; Cheung, K.F. Depth-integrated free-surface flow with parameterized non-hydrostatic pressure. *Int. J. Numer. Methods Fluids* **2013**, *71*, 403–421. [CrossRef]
28. Cui, H.; Pietrzak, J.D.; Stelling, G.S. Optimal dispersion with minimized Poisson equations for non-hydrostatic free surface flows. *Ocean. Model.* **2014**, *81*, 1–12. [CrossRef]
29. Tarwidi, D.; Pudjaprasetya, S.R.; Adytia, D. A reduced two-layer non-hydrostatic model for submarine landslide-generated tsunamis. *Appl. Ocean. Res.* **2022**, *127*, 103306. [CrossRef]
30. Walters, R.A. A semi-implicit finite element model for non-hydrostatic (dispersive) surface waves. *Int. J. Numer. Methods Fluids* **2005**, *49*, 721–737. [CrossRef]
31. Pudjaprasetya, S.R.; Magdalena, I.; Tjandra, S.S. A Nonhydrostatic Two-Layer Staggered Scheme for Transient Waves due to Anti-Symmetric Seabed Thrust. *J. Earthq. Tsunami* **2017**, *11*, 1740002. [CrossRef]
32. Nwogu, O. Alternative Form of Boussinesq Equations for Nearshore Wave Propagation. *J. Waterw. Port Coastal Ocean. Eng.* **1993**, *119*, 618–638. [CrossRef]
33. Lo, H.Y.; Liu, P.L.F. On the analytical solutions for water waves generated by a prescribed landslide. *J. Fluid Mech.* **2017**, *821*, 85–116. [CrossRef]
34. Whittaker, C.; Nokes, R.; Davidson, M. Tsunami forcing by a low Froude number landslide. *Environ. Fluid Mech.* **2015**, *15*, 1215–1239. [CrossRef]
35. Jing, H.; Chen, G.; Liu, C.; Wang, W.; Zuo, J. Dispersive effects of water waves generated by submerged landslide. *Nat. Hazards* **2020**, *103*, 1917–1941. [CrossRef]